Macromolecules

pubs.acs.org/Macromolecules

Article

Long Tails with Flower-like Conformations Undergo an Escape Transition in Homopolymer Adsorption Layers

Frans A.M. Leermakers*

Cite This: *Macromolecules* 2020, 53, 3900−3906

Read Online

ACCESS | Metrics & More | Article Recommendations

ABSTRACT: De Gennes predicted that homopolymer adsorption on a solid−liquid interface results in an adsorption profile with a proximal, a central, and a distal region, wherein, for a good solvent, the central region has a self-similar structure with a density profile that decays as a power law with a coefficient of −4/3. Recent numerical self-consistent field (SCF) predictions for the long-chain length (N) limit revealed a more complex central region with an inner part, where the loops dominate the layer, with a (mean-field) power-law coefficient of −2 and an outer part, where tails dominate, with a "de Gennes" scaling of −4/3. The tails with length $t < t^*$ contribute to the inner part of the central region, and these have similar conformations as the loops. The outer part is populated by tails with a length $t > t^*$, and these behave differently. With the increasing length of the tails, there exists a weak escape transition at $t = t^{escape} \approx N/10$. Long tails in the adsorption profile ($t \gtrsim t^* \propto N^{0.733}$) show enhanced fluctuations due to this nearby escape transition, and this explains the excluded volume scaling for the outer part of the central region in SCF. With this interpretation, the −2 scaling found by SCF for the inner part should be classified as a mean-field result.

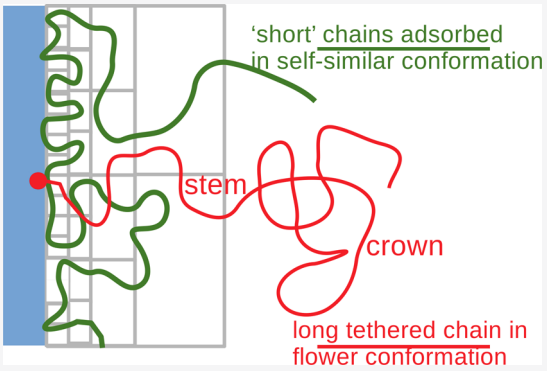

INTRODUCTION

Long polymer chains strongly adsorb onto solid−liquid interfaces already from very low concentrations when the adsorption energy per segment exceeds a critical value.[1,2] De Gennes was the first to recognize that the adsorption profile has many universal properties.[3] We focus on strong adsorption for which de Gennes predicted that the adsorbed layer naturally splits up into three regions. (i) The proximal region near the surface has a volume fraction close to unity $\varphi \sim 1$, and the width of this layer is smaller when the adsorption energy is higher. For strong adsorption, the proximal zone becomes of the segment size. (ii) Next to this, there exists a central region wherein the polymer density is in the semidilute regime. For this, de Gennes predicted that the layer has a self-similar structure. His arguments are transparent. In line with experiments, de Gennes noticed that, in the semidilute solutions, there exists a correlation length ξ, which depends on the concentration $\xi \propto \varphi^{-3/4}$. He then realized that, in the adsorption layer, the local correlation length becomes limited to the distance to the surface z, and by equating the correlation length to this distance, he obtained directly the density profile $\varphi(z) \propto z^{-4/3}$. (iii) In the periphery of the adsorption layer, the distal region, the density of adsorbed segments drops below the overlap concentration. For this part of the profile, an exponential decay of the segment density was predicted, wherein the decay length is given by the coil size.

Early numerical self-consistent field modeling by the Scheutjens−Fleer method (SF-SCF) confirmed the proximal-central-distal picture for the adsorption profile.[4] However, the central region was found to have a "mean-field power-law" coefficient: $\varphi(z) \propto z^{-2}$. For these computations chains with length, $N = 5 \times 10^{-4}$ was used. Small irregularities near the crossover from the central to distal regions were ignored at that time. More recent calculations,[5] which were executed for molecular weights up to $N = 5 \times 10^6$ (two decades more than the earlier computations), proved that, in SCF, the central region has a more complex structure. An inner part of the central region the mean-field power-law coefficient of −2 was found, while in the outer part of the central region, the "de Gennes", excluded volume, coefficient of −4/3 was recovered (in the limit of infinitely long chains). These results should still be classified as "surprising" because the excluded volume (de Gennes) scaling was not expected to show up in SF-SCF modeling.

Joanny and Semenov[6] analyzed the loop and tail structure of the adsorption profile in a two-order parameter analysis. They

Received: February 17, 2020
Revised: April 22, 2020
Published: May 13, 2020

https://dx.doi.org/10.1021/acs.macromol.0c00361
Macromolecules 2020, 53, 3900−3906

found that, even though the loops and tails behave differently, they contribute in the same manner to the adsorption profile, that is, the sum of the loops and tails gave the overall profile $\varphi(z) \propto z^{-2}$. This motivated Aubouy and co-workers[7] to forward a scaling analysis of the polymer adsorption layer based upon the loop size distribution, that is, the number of loops with length t, $n^{\text{loop}}(t)$; in fact, these authors use the integrated variant only. They used $n^{\text{loop}}(t) \propto t^{-11/5}$, a result predicted earlier by de Gennes,[8] and completely ignored the presence of tails.

In this paper, we will present SF-SCF predictions for the loop and tail conformations within the polymer adsorption layer for long chains in a good solvent, adsorbing from dilute solutions. Most of our results are for $N = 10^5$, which is just enough to see a reasonable sized outer part of the central region, but of course, these chains are not long enough yet to find the −4/3 coefficient accurately. The chain length dependence has been examined in detail in our previous work,[5] and we will not repeat this here. For $N = 10^5$, we were able to analyze the loop and tail size distribution. Not unexpectedly, we see that these distributions have power-law characteristics both for fragment lengths that contribute to the inner and outer part of the central region. When we add up these distributions, more precisely when we add to the loop distribution half the tail distribution (two tails make up one loop), we recover the size distribution consistent with the de Gennes predictions.

We then focused on the distribution of the tails with length (t) and recorded the overall volume fraction profile of tails with a specified length t and the corresponding end-point distribution $g_t(z)$. Such analysis is routinely done for polymer brushes[9−11] but never performed for tails in the polymer adsorption profile. We argue that the tails have an inhomogeneous conformations, which may be referred to as flower-like conformations. These inhomogeneous conformations are characterized by a stem and a crown.[12,13] In this case, the stem originates at the surface and the zone in which the stem resides grows with the square root of the tail length; the crown exists at larger z coordinates. With increasing length of the tails, we find an "escape" transition; when tails are long enough to escape from the adsorption layer, they stretch on average a bit more to probe the region outside the layer. Such escaped flowers are best recognized by considering tails that are longer than the length of the chains that made the adsorbed layer, i.e., for $t > N$, in the limit of long chains N. We refer to the TOC graphics for an illustration of the escape transition effect.

Inhomogeneous flower-like conformations are complicating the analytical mean-field analysis of polymer brushes. Indeed, the applicability of analytical mean-field theories is formally restricted to systems wherein the end-point distribution does not show the so-called dead zone: regions near the surface where the end point is not allowed to reside because the analytical end-point distribution can turn negative for such situations.[14] Flower conformations do have an end-point distribution with a dead zone. Also, for analytical polymer adsorption models, the existence of inhomogeneous conformations, that is, flower-like conformations of the tails, pose a serious challenge to analytical modeling. It turns out that sufficiently long flower-like tails can escape from the adsorption layer. They appear to do so in a cooperative manner. Joanny and Semenov[6] did not consider the option of an escape transition of some sort, which may explain why these authors found that the outer part of the central regime was also following the mean-field scaling with a coefficient of −2. Below, we will argue that the tails with lengths comparable to the critical length, where the escape transition takes place, experience enhanced fluctuations. These more strongly fluctuating tails may have contributed to the de Gennes-like scaling coefficient, approaching a value of −4/3 in the limit of long chains.

SCHEUTJENS−FLEER SELF-CONSISTENT FIELD THEORY

At the basis of the SF-SCF approach[2,15,16] is a mean-field free energy functional wherein two conjugated distributions are present, namely, (i) the segment densities $\varphi(z)$ and (ii) the segment potential $u(z)$. Such pair of distributions exists both for the polymer segments as well as for the solvent. We will use the subindex p for the polymer and the subindex S for the solvent. The optimization of this free energy functional leads to (i) a rule how to compute the volume fraction profiles from the corresponding segment potentials and (ii) a rule how to compute the segment potentials from the volume fraction profiles. These rules should be implemented, while the system is incompressible, that is, that for each coordinate z, the sum of the densities equals unity, i.e., $\varphi_p(z) + \varphi_S(z) = 1$.

(i) To compute the densities from the potentials that require an appropriate chain model, as usual, the Edwards diffusion equation[17] is used

$$\frac{\partial G(z, s)}{\partial s} = \frac{1}{6}\frac{\partial^2 G(z, s)}{\partial z^2} - u(z)G \tag{1}$$

which is applicable for Gaussian chains in a potential field $u(z)$. In the SF-SCF method, this differential equation is mapped on a discrete set of coordinates $z = 1, 2,..., M$ next to a solid substrate that resides in the other half-space $z < 1$, and the contour length parameter s is redefined as a segment ranking number $s = 1, 2,..., N$ with N being the total number of Kuhn segments in the chain. In this process, the chain model transfers into a freely jointed chain model on a discrete lattice. Typically, the Edwards equation requires initial conditions, and application of these initial conditions are usually reflected in the notation of the end-point distribution G. Similarly, in the SF-SCF approach, initial conditions are needed. Using the potentials, we can define the so-called free segment distribution function $G_p(z) = \exp(-u_p(z))$ where we have normalized the potentials by the thermal energy k_BT. Using initial conditions $G_p(z, 1|1) = G_p(z)$, one can compute an arbitrary end-point distribution $G_p(z, s|1)$ using the recurrence relation

$$G_p(z, s|1) = G_p(z)\langle G_p(z, s - 1|1)\rangle \tag{2}$$

where the site fraction $\langle G_p(z, s - 1|1)\rangle$ encompasses a three-layer average

$$\langle G_p(z, s|1)\rangle = \lambda_1 G_p(z - 1, s|1) + \lambda_0 G_p(z, s|1) + \lambda_1 G_p(z + 1, s|1) \tag{3}$$

Here, $\lambda_0 = 1 - 2\lambda_1$ is the fraction of "neighbors" that a site has within sites in the same layer, whereas λ_1 is the fraction of neighbors that a site has with a previous or next layer. Typically, a cubic lattice is assumed for which $\lambda_1 = 1/6$. Although, in relation to the Edwards equation, this seems to be the logical value for λ_1, and we now believe that the better choice is $\lambda_1 = 1/4$, that is, the value for a hexagonal lattice is more appropriate.[18] Hence, we use this latter value throughout this paper. It must be understood that all results are qualitatively the same, irrespective using 1/4 or 1/6 for this parameter, and only, quantitatively, the

https://dx.doi.org/10.1021/acs.macromol.0c00361
Macromolecules 2020, 53, 3900−3906

results differ. A detailed motivation for the choice of a hexagonal lattice will be published elsewhere.

The volume fraction is found by the composition law. For symmetric polymers, for which for all values of the segment ranking number s, the segment with ranking number s is of the same type as the segment with the ranking number $N - s + 1$, we have

$$\varphi_p(z) = \varphi_p^b \sum_{s=1}^{N} \frac{G_p(z, s|1) G_p(z, N - s + 1|1)}{G_p(z)} \tag{4}$$

where the division by $G_p(z)$ is required to correct for double counting of the segment weight for segment s.

The volume fraction distribution of the (monomeric) solvent is found by $\varphi_S(z) = (1 - \varphi_p^b)\, G_S(z)$.

(ii) Computing the potentials from the segment densities requires a choice on how interactions between molecules are accounted for. For this, the Flory–Huggins/regular solution approach is followed, which quantifies the interactions using the Flory–Huggins interaction parameter χ and implements a mean-field approach wherein the number of contacts are evaluated using the volume fractions[19]

$$\begin{aligned} u_p(z) &= \alpha(z) + \chi(\langle \varphi_S(z) \rangle - \varphi_S^b) + \delta_{z,1} \chi_s \lambda_1 \\ u_S(z) &= \alpha(z) + \chi(\langle \varphi_p(z) \rangle - \varphi_p^b) \end{aligned} \tag{5}$$

Here, the angular brackets again implement a three-layer average as, in eq 3, it is the characteristic for the SF version of the SCF theory for polymeric systems. The kronicker $\delta_{z,1} = 1$ when $z = 1$ and 0, otherwise makes sure that the adsorption energy is only used for segments next to the solid boundary. χ_s quantifies the adsorption energy, which is defined with opposite sign as the classical Silberberg adsorption parameter.[20] The value is chosen with respect to the solvent adsorption energy (which is set to zero). A negative value for χ_s means that the segment gains energy upon exchange with a solvent next to the substrate. Typically when χ_s is less than -1, the adsorption is strong enough to overcome the entropy loss of chain bonds next to the substrate. The χ is the solvency parameter. Athermal solvent, also called a good solvent, is characterized by $\chi = 0$. The ideal solution, or the theta solvent, requires a value of $\chi = 0.5$. For the latter choice, the segment second virial coefficient, $\beta = 1 - 2\chi$, is equal to zero. Finally, in eq 5, the quantity α is a contribution to the segment potential required to generate space for the segment/solvent monomer. The value is adjusted, in the numerical scheme that is followed to find the SCF solution, such that the incompressibility condition applies.

The self-consistent field solution requires the two rules to be at a stationary point. That is, the potentials that determine the volume fractions are recomputed from these volume fractions. Also the reverse is true. The volume fractions that determine the potentials are recomputed from these potentials. This fixed point is found routinely by an iterative procedure with a significance of at least seven significant digits.[21]

For such an SCF solution, one can evaluate the loop and tail size distribution, as explained extensively in the literature.[16] The profile for a tail with length t is also easily evaluated. For this, we first compute the SCF solution and the $u_p(z)$ profiles are exactly known (and fixed). Hence, also, $G_p(z)$ is available. We implement initial conditions $G_t(1, 1|1) = G_p(z)$ and set $G_t(z, 1|1) = 0$ for $z > 1$. Then, the propagator (eq 2) is slightly modified to avoid that the chain fragment visits the surface layer more than once

$$G_t(z, s|1) = \begin{cases} G_p(z)\langle G_t(z, s - 1|1) \rangle & z > 1 \\ 0 & z = 1 \end{cases} \tag{6}$$

which obviously is used for $s = 2,\ldots,t$. Note that, in the adsorption layer, the longest tail is $t = N$. However, nothing prevents us to also consider the profile of tails that are longer than N. The end-point distribution of the tail with length t is available as $g_t(z) = G_t(z, t|1)$. The overall distribution of tails with length t can only be computed with the aid of a second set of end-point distribution functions. We start these by the free end $s = t$

$$G_t(z, t|t) = \begin{cases} G_p(z) & z > 1 \\ 0 & z = 1 \end{cases} \tag{7}$$

and propagated similarly as above. Again, we need to avoid that chains visit the layer $z = 1$, except for the very last segment

$$G_t(z, s|t) = \begin{cases} G_p(z)\langle G_t(z, s + 1|t) \rangle & z > 1 \text{ and } s > 1 \\ G_p(z)\langle G_t(z, s + 1|t) \rangle & z = 1 \text{ and } s = 1 \\ 0 & z = 1 \text{ and } s \neq 1 \end{cases} \tag{8}$$

and the distribution of tails with length t follows from the composition law

$$\varphi_t^{\text{tail}}(z) = C \sum_{s+=1}^{t} \frac{G_t(z, s|1) G_t(z, s|t)}{G_p(z)} \tag{9}$$

The normalization C is chosen such that $\sum_{z=1}^{M} \varphi_t(z) = 1$.

The overall volume fraction profile of loops with length l can be evaluated similarly. We may compute the end-point distributions basically generated by eq 6, slightly modified for the propagation toward the last segment: the end-point distribution for the last segment t may only have a non-zero value for $z = 1$. Realizing that loops are symmetric, the first and last segments must reside in layer $z = 1$, and all other segments cannot enter this coordinate, we find

$$\varphi_l^{\text{loop}}(z) = C \sum_{s=1}^{l} \frac{G_t(z, s|1) G_t(z, l - s + 1|1)}{G_p(z)} \tag{10}$$

and again, C can be chosen such that the distribution is normalized to unity.

RESULTS AND DISCUSSION

Evaluation of the polymer adsorption profile in the high chain length limit is computationally challenging.[5] Due to a computational inexpensive propagator formalism to generate the single chain partition function, the SF-SCF computations are feasible for chains that exceed a length of $N = 10^6$, but due to the CPU time needed for these computations, it is not practical to consider these routinely. Most features can already be well recognized for shorter chains. That is why, by default, we will choose to use $N = 10^5$. The solvent strength by default is taken to be athermal. For this case, the nontrivial result exists for the polymer adsorption profile. For the theta conditions, there is more consensus of what to expect. We will focus on the case that the adsorption energy per segment exceeds by far the critical value, and by default, a segment near the adsorbing surface experiences 1 $k_B T$ adsorption energy. In a hexagonal lattice with

https://dx.doi.org/10.1021/acs.macromol.0c00361
Macromolecules 2020, 53, 3900−3906

$\lambda_1 = 1/4$, this means that $\chi_s = -4$. Typically, we will assume that the polymers adsorb from a dilute solution near the overlap concentration. Again, by default, we have implemented $\varphi_p{}^b = 1/N$.

Let us start by presenting the overall density profile $\varphi_p(z)$ for the default case in combination with the overall tail and loop distributions. As can be seen in Figure 1, the overall profile has a

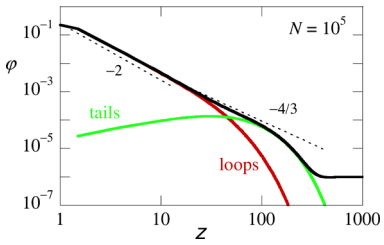

Figure 1. Volume fraction profile in double logarithmic coordinates for the case $N = 10^5$, good solvent $\chi = 0$, strong adsorption $\chi_s = -4$, hexagonal lattice $\lambda_1 = 1/4$, and bulk volume fraction $\varphi_p{}^b = 10^{-5}$. The overall distribution of the loops and the tails are also given. The dotted lines represents local trends of the overall profile. The numerical values near these lines are an estimate of the slope of the respective dotted lines.

pronounced central region, which extends in this case from $2 < z < R_g \sim 110$. As the adsorption energy is high, the proximal region is reduced to just one lattice layer. The distal region has an exponential distribution (not shown) and extends $\sim 110 < z < \sim 400$. At the periphery of the adsorption layer, there is a depletion zone where freely dispersed chains of the bulk do enter with a low frequency. This depletion zone is best visible when the bulk concentration is near the overlap. In the same figure, the overall loop and tail volume fraction profiles are plotted. Clearly, the tails are dominant in the outer part of the profile, whereas the loops dominate at the inner region. The tail and loop distributions cross at coordinate z^*, which is known to scale with the chain length as $z^* \propto N^{1/3}$.[22] For $z < z^*$, the density profile follows $\varphi(z) \propto z^{-2}$ to a very good approximation. We call this the inner part of the central region. In the outer part $z^* < z < R_g$, the profile approaches $\varphi(z) \propto z^{-4/3}$. This is better judged from a local power-law slope computed from $\alpha_{z'} = (\partial \log \varphi(z)/\partial \log z)_{z=z'}$. From this information (not shown), it can be concluded that the $-4/3$ coefficient is not yet reached for $N = 10^5$. Better results are obtained for chains that are 10−100 times larger.[5] We will not pursue this issue here further as it was the topic of the mentioned paper.

The key issue is to explain why, in the SF-SCF method, the central region splits up into two subregions, an inner and outer part. It has been suggested[5] that, in the inner part wherein loops dominate the profile and a local "blob" is "populated" by two chain parts, one goes away from the surface and one is coming toward the surfaces. Such a blob was suggested to be overcrowded and therefore has mean-field characteristics. The blobs in the tail-dominated region only contains chain fragments that go away from the surface and, following the arguments, these blobs could show excluded volume scaling. However, such a heuristic argument is hard to underpin and our hope is that more insights in the structure of the adsorption layer may be found from a more detailed analysis. Results presented in this paper reveal an alternative view on the adsorption layer.

It is generally believed that the loop size distribution plays a pivoting role in the polymer adsorption profile.[7] It is expected that such size distribution has power-law features when the chain length is long. Predictions for these distributions have been reported for rather short chains only[16] and that is why it is here of interest to present these distribution for the $N = 10^5$ case. In Figure 2, we present these results both for good and theta

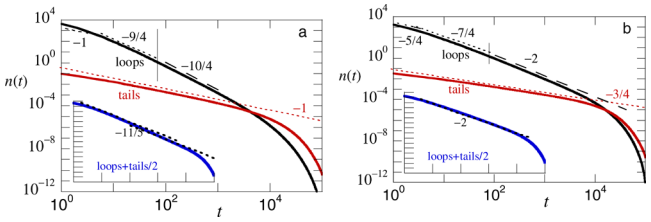

Figure 2. Loop $n^{loop}(t)$ and the tail size distribution $n^{tail}(t)$ in double logarithmic coordinates. In the inset, the added distribution $n^{tot}(t) = n^{loop} + \frac{1}{2}n^{tail}$ is presented on the same scale. The dashed and dotted lines are the (shifted) power-law fits, and the number near the lines present the estimated slope of the fit. (a) Good solvent and (b) theta solvent.

solvents (Figure 2a b, respectively). Inspection of these graphs show that, for the tail distribution, a better overall power-law fit is possible. The loop distribution has some curvature, and a trial fit for short fragment lengths t leads to a slightly different exponent as for longer lengths. Adding both tail and loop distributions (tail is counted as half a loop), leads, for good solvents, to a power-law fit are close to the result found by de Gennes[8] and used by Aubouy and co-workers,[7] namely, $n^{tot}(t) \propto z^{-11/5}$. This result is found to a reasonable approximation both for small and large values of t (note that, numerically, it is hard to differentiate between $-11/5$ and $-9/4$). There seems to be a small crossover region for which the $-11/5$ value is not followed (in between long and short fragment lengths, i.e., for $t \sim 100$). For the theta solvent, the overall length distribution of the loops plus that of the tails leads to a coefficient of -2 to a good approximation.

One can define a crossover fragment length t^*: for $t < t^*$, there are more loops of length t than tails of length t. The reverse is true for $t > t^*$. For $N = 10^5$, we find $t^* \approx 4200$. Fitting this crossover length for $10^3 < N < 10^5$ indicates a good power-law scaling of $t^* \approx 0.909N^{0.733}$. For the theta solvent, the crossover length is much higher $t^* \approx 0.577N^{0.89}$.

Realizing that, for good solvents, the tail size distribution dominates over that of the loops, and it is of interest to scrutinize the tail properties in more detail. For this reason, we decided to consider the overall volume fraction profile for tails with a specified length t, $\varphi_t{}^{tail}(z)$ as well as the corresponding distribution of the ends given by $g_t{}^{tail}(z)$. Comparing long and short tails in one graph requires some normalizations: (i) we adjusted the normalization of the profiles such that they all have the same maximum value of unity. (ii) Furthermore, the tails are not strongly stretched, and therefore, they extend not much with respect to the Gaussian size. That is why the profiles closely match when the z coordinate is normalized by $\sqrt{t}$.

In Figure 3, we show the profiles for $t = 10^5$ (which is the longest possible tail in the adsorption layer) as well as for tails that are significantly shorter, i.e., for $t = 10^3$ and 10^4. These profiles are recorded for the adsorption profile generated by adsorbing chains with length $N = 10^5$. Upon first inspection, the profiles are very similar. The overall profile for the longer tail is a bit narrower, and the density near the surface is relatively suppressed. The corresponding end points also deviate a little. It seems that the end points of the longest tails avoid the surface

https://dx.doi.org/10.1021/acs.macromol.0c00361
Macromolecules 2020, 53, 3900−3906

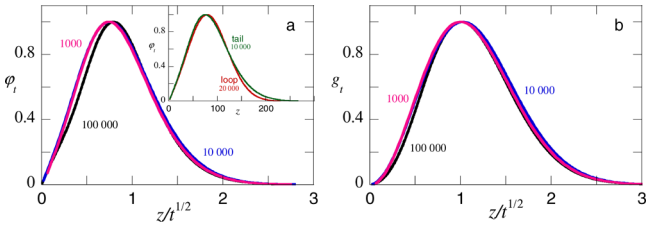

Figure 3. (a) Overall volume fraction profiles. (b) Corresponding end-point distributions for tails with length $t = 10^3$, 10^4, and 10^5 in a adsorption layer of chains with length $N = 10^5$ (default system). The distance to the wall is normalized by $\sqrt{t}$ and for all profiles that are maximum is normalized to unity. In the inset of panel (a), the overall volume fraction profile is given for loops with $t = 2 \times 10^4$ and tails with half this length, i.e., $t = 10^4$.

layer a bit more than the short tails. We should realize that, in real space, the growth of the zone near the surface wherefore the ends of the tails are depleted is growing with t. The reason for this growth lays in the definition of the tails. When end-tethered chains would have been allowed to revisit layer $z = 1$, the end-point distribution would not have featured the same reduced probability near the surface. However, a part of this end-tethered chain is lost as these parts did form "loops" of some kind and are not counted as tails. Of course, the tails cannot return to $z = 1$, and already, the smallest tail has a dead zone with size unity. As all end-point distributions of Figure 3b are almost on top of each other while plotted as a function of $z/\sqrt{t}$ means that the dead zone grows proportional to $\sqrt{t}$ (see also Figure 4b below).

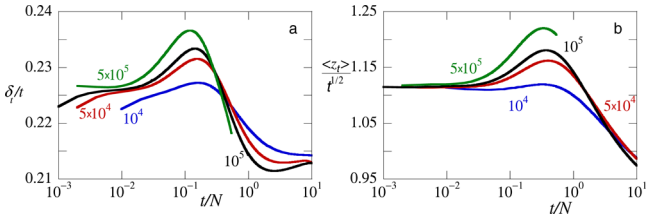

Figure 4. (a) Relative fluctuations δ_t/t of the end group of tails with length t versus the reduced length of the tail t/N, for different values of the length of the chains N in the adsorption layer in lin-log coordinates. (b) Corresponding average position of the end segment of a tail with length t normalized by the square root of t versus the reduced length t/N in lin-log coordinates. Parameters: ${\varphi_p}^b = 1/N, \chi = 0, \chi_s = -4$, and $\lambda_1 = 1/4$.

The tail with length $t = N$ in practice hardly occurs of course, and therefore, this profile is not that relevant for the overall profile. More of interest for the profile are tails that are larger than t^* but not too much. The $t = 10^4$ tail, also shown in Figure 3, is a representative of these more relevant tails. As can be seen, for these tails, a relatively wide overall density profile and a wide end-point distribution is recorded. We argue that these small changes are early signals for an escape transition.

In passing, we mention that it is often assumed that loops can be approximated by two tails with half the chain length. In the inset of Figure 3a, we therefore show the overall profiles for tails with length $t = 10^4$ (which is larger than t^*) and loops with double this chain length $t = 2 \times 10^4$. In these profiles, the density is given as a function of z and it is clear that the tail samples have larger z values than the loops. In fact, the distribution of the tail is wider than that of the double-sized loop. Again, it is hard to say at this point whether or not this difference is significant enough to explain the excluded volume scaling found in the tail-rich region.

A systematic way to quantify tail conformations is to record the fluctuations of the end points. Therefore, we first evaluate the first and second moments of the end-point distribution of tails with length t, which are found by

$$\langle z_t^x \rangle = \frac{\sum_{z=1}^{M} (z - 0.5)^x g_t(z)}{\sum_{z=1}^{M} g_t(z)} \tag{11}$$

for $x = 1$ and 2, respectively. The shift of the z coordinate by 0.5 is not very important but is motivated by the fact that a segment in layer z is a distance of $z - 0.5$ away from the surface. The relative fluctuations of a tail with length t is then given by

$$\frac{\delta_t}{t} = \frac{\langle z_t^2 \rangle - \langle z_t^1 \rangle^2}{t} \tag{12}$$

In Figure 4, we present relative fluctuations of the tails with length t and the corresponding normalized average position of the tail end as a function of the reduced tail length t/N, for adsorption layers with chains of length $N = 5 \times 10^4$,..., 5×10^5. For the lower molecular weights, we have extended the range of tail lengths beyond the length of the polymers that formed the adsorption layer, that is, $t > N$. The fluctuation curves that are found are characterized by a "plateau" with $\delta_t/t \approx 0.226$ for short tails $t/N \sim 0.01$ and a lower plateau for $t/N > 10$. In between these limits, the relative fluctuations go through a maximum. Obviously, this maximum is still tiny for the presented values of N, but its height is systematically increasing with the increasing chain length N. Such dependence is expected for finite-size effects affecting a phase transition. The reduced average positions (cf. Figure 4b) also go through a clear maximum (at slightly larger values for t/N). These reduced averages go through a weaker minimum for small t values and drop to low values for large values of t.

Considering the trends discussed above, we argue that the escape phase transition is causing the mentioned increase in the fluctuations. In Figure 5, we show the end-point distributions for

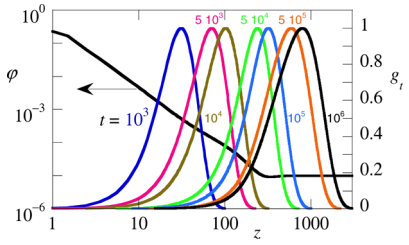

Figure 5. Illustration of tail conformations in relation to the overall density profile. The left ordinate is the logarithm of the overall volume fraction profile (for reference only) for $N = 10^5$. The right ordinate is the end-point distribution of the tails with length t, i.e., $g_t(z)$. Both profile types are given for as a function of z in logarithmic coordinates. The values of t are indicated.

tails for a wide range of t values to elaborate on this escape transition. In this case, we plot these results as a function of z. From these profiles, we see that all tails have a dead zone as already noticed above and that the width of the dead zone increases with t, $t > N$ the width of the dead zone saturates. This last point is seen from the two profiles $t = 5 \times 10^5$ and 5×10^6; both profiles start to have significant values at approximately the same z coordinate.

https://dx.doi.org/10.1021/acs.macromol.0c00361
Macromolecules 2020, 53, 3900−3906

From Figure 4a, we can see that the escape transition occurs at approximately $t \equiv t^{escape} \approx N/10$ (t^{escape}/N seems to decrease with increasing N). The flower that has grown outside the adsorption layer has, as mentioned already, a fixed stem length (equal to the dimensions of the adsorption layer) and a weakly deformed crown. As the ends of the tail reside in the crown of the flower, the fluctuations of the end points are restricted in the crown region. This causes the fluctuations to be relatively low for tails that have escaped from the adsorption layer. The fluctuations do recover of course when, with increasing t,more segments can take place in the crown, and the fraction of segments in the stem goes down (hence, the fluctuations go trough a minimum near $t \approx N$).

In the other extreme where the tail is buried in the adsorption layer, the stem is relatively short (it is in the growing regime with t) and the crown exists in most of the central region of the profile. The relative fluctuations for these short tails are a bit larger than the relative fluctuations of the longest tails. This might be due to the fact that the crown is in a potential gradient of the adsorbed chains and therefore slightly stretched.

For intermediate tail lengths, near the escape transition, the tails are still inside the adsorption layer, but they start to sample the outer space outside the adsorption profile. They stretch a bit to do so. This is seen by the fact that the average position of the ends normalized by the square root of its length, going through a local maximum (cf. Figure 4b). At the same time, their fluctuations are relatively high. As the maximum in δ_t/t increases for larger values of N, we expect that, in the limit of $N \to \infty$, we will find δ_t to diverges. For the chain lengths sampled in Figure 4, we are still far from this limit; indeed, the escape transition is weak because there are only small quantitative changes in the type of conformations of the tails. Interestingly, the escape transition is of an excluded volume type and the enhanced fluctuations that are picked up by tails of intermediate length may be identified as excluded volume fluctuations.

The longest relevant tail in the adsorption layer may be close to $t \approx 10 \times t^*$. That means that, typically, the tails that matter for the profile are smaller than t^{escape}. However, these intermediate length tails are already experiencing enhanced fluctuations that are caused by the nearby transition. We argue that these enhanced fluctuations are causing the de Gennes-like scaling exponent resembling $-4/3$ in the outer part of the central region.

This suggestion has implications for the rationalization of the SF-SCF results for polymer adsorption. Typically, one expects that, in SF-SCF, excluded volume correlations are missing, and therefore, the method can only predict mean-field power-law coefficients. Yet, the SF-SCF method produced the $-4/3$ power-law coefficient in the outer part of the central region. We now understand that, within the SF-SCF modeling, there are possibilities that excluded volume fluctuations can affect the profile: there exists an escape transition of long tails with flower-like conformations. Short flower-like tails tails are completely confined within the adsorption layer. Long tails can stretch their stem in the z direction in an attempt to bring the crown outside the adsorption layer. This escape transition introduces enhanced fluctuations for tails in the z direction (for long tails in the proximity of the transition point), and this allegedly leads to a higher than mean-field power-law coefficient in the outer part of the central region. Of course, in reality, the polymer chains in a good solvent should show excluded volume correlations throughout the central region of the adsorption layer and not only in the outer part of it. In SF-SCF, the inner part of the central region is not influenced by the escape transition because the loops dominate in this region, and therefore, the mean-field power-law coefficient for the density profile is the natural (flawed) result. We can thus return to the classical picture for polymers at interfaces: one can use the SCF predictions to illustrate the proximal-central-distal picture of the adsorption layer and then implement a switch of the power-law coefficient from -2 to $-4/3$ to account for the excluded volume correlations. This switch of coefficients is not needed for the outer part of the central region because this part is already in accordance of the de Gennes picture.

As a final remark, it must be clear that we do not recommend experiments to catch specifically the mentioned coil-to-flower transition for long tethered chains in the adsorption profile. Arguably, this transition only exists in a mean-field world. In reality, the excluded volume fluctuations exist throughout the central region of the profile, i.e., also in the lateral directions along the interface. Then, also, the inner part of the central region has the $-4/3$ scaling and typical escape effect due to excluded volume effects occurring throughout the layer. Apart from this, experiments that show that long tethered chains can escape from an adsorption layer of shorter chains are of course of interest as such composite layers may be used in biosensors or drug delivery applications.

CONCLUSIONS

Numerical self-consistent field calculations for polymers strongly adsorbing onto the solid−liquid interface from a good solvent reveals a complex structure of the central region with two power-law subregions. (i) The inner part has a mean-field scaling exponent of -2. We now expect that, when excluded volume correlations are included, this value should be replaced by $-4/3$. (ii) Surprisingly, the outer part of the central region was already found to give a scaling exponent close to $-4/3$. We now argue that a nearby escape phase transition causes an increase in excluded volume fluctuations of long tails in flower-like conformations such that the power-law coefficient could be increased from -2 to $-4/3$. The escape phase transition takes place for tails with increasing tail lengths t at a threshold t^{escape} with $t^{escape} \approx N/10$. This weak transition can be noticed for large N values only, and this explains why, in the mean-field results, the $-4/3$ power-law coefficient shows up only in the high chain length limit. In reality, we expect $-4/3$ coefficients also for adsorption layers composed of short chains.

AUTHOR INFORMATION

Corresponding Author

Frans A.M. Leermakers − *Physical Chemistry and Soft Matter Wageningen University, Wageningen, WE 6708, The Netherlands;* orcid.org/0000-0001-5895-2539; Email: frans.leermakers@wur.nl

Complete contact information is available at: https://pubs.acs.org/10.1021/acs.macromol.0c00361

Notes

The author declares no competing financial interest.

REFERENCES

(1) Lyklema, J. *Fundamentals of Interface and Colloid Science*; Academic press: London, 1991.

(2) Fleer, G. J.; Scheutjens, J. M. H. M.; Cohen-Stuart, M. A.; Vincent, B.; Cosgrove, T. *Polymers at interfaces*; Chapman and Hall; London-Glasgow 1993.

https://dx.doi.org/10.1021/acs.macromol.0c00361
Macromolecules 2020, 53, 3900−3906

(3) de Gennes, P.-G. Polymer-solutions near an interface. adsorption and depletion layers. *Macromolecules* **1981**, *14*, 1637−1644.
(4) Van der Linden, C. C.; Leermakers, F. A. M. On the self-similar structure of adsorbed polymer layers: dependence of the density profile on molecular weight and solution concentration. *Macromolecules* **1992**, *25*, 3449−3453.
(5) Leermakers, F. A. M. Self-consistent field modeling of homopolymers at interfaces in the long chain length limit. *Polym Sci. Ser. C* **2018**, *60*, 18−24.
(6) Joanny, J.-F.; Semenov, A. N. Structure of adsorbed polymer layers-loops and tails. *Europhys. Lett.* **1995**, *29*, 279−284.
(7) Aubouy, M.; Guiselin, O.; Raphaël, E. Scaling description of polymer interfaces: flat layers. *Macromolecules* **1996**, *29*, 7261−7268.
(8) de Gennes, P.-G. Weight distribution of loops in a diffuse, adsorbed polymer layer. *C.R. Acad Sci., Paris II* **1982**, *294*, 1317.
(9) Semenov, A. N. Contribution to the theory of microphase layering in blockcopolymer melts. *Sov. Phys. JETP* **1985**, *88*, 1242.
(10) Milner, S. T.; Witten, T. A.; Cates, M. E. Theory of the grafted polymer brush. *Macromolecules* **1988**, *21*, 2610−2619.
(11) Zhulina, E. B.; Priamitsyn, V. A.; Borisov, O. V. Structure and conformational transitions in grafted polymer-chains layers - new theory. *Polymer Science USSR* **1989**, *31*, 2−5.
(12) Subramanian, G.; Williams, D. R. M.; Pincus, P. A. Escape transitions and force laws for compressed polymer mushrooms. *Europhys. Lett.* **1995**, *29*, 285−290.
(13) Skvortsov, A. M.; Klushin, L. I.; Leermakers, F. A. M. Exactly solved polymer models with conformational escape transitions of a coil-to-flower type. *Europhys. Lett.* **2002**, *58*, 292−298.
(14) Wijmans, C. M.; Zhulina, E. B. Polymer brushes at curved surfaces. *Macromolecules* **1993**, *26*, 7214−7224.
(15) Scheutjens, J. M. H. M.; Fleer, G. J. Statistical theory of the adsorption of interacting chain molecules. 1. partition function, segment density distribution, and adsorption isotherms. *J. Phys. Chem.* **1979**, *83*, 1619−1635.
(16) Scheutjens, J. M. H. M.; Fleer, G. J. Statistical theory of the adsorption of interacting chain molecules. 2. train, loop and tail size distribution. *J. Phys. Chem.* **1980**, *84*, 178−190.
(17) Edwards, S. F. The statistical mechanics of polymers with excluded volume. *Proc. Phys. Soc.* **1965**, *85*, 613−624.
(18) Egorov, S. A.; Romeis, D.; Sommer, J. U. Surface instabilities of minority chains in dense polymer brushes: A comparison of density functional theory and quasi-off-lattice self-consistent field theory. *J. Chem. Phys.* **2012**, *137*, No. 064907.
(19) Flory, P. J. *Principles of Polymers Chemistry*; Cornell University Press: Ithaca, NY, 1953.
(20) Silberberg, A. Multilayer adsorption of macromolecules. *J. Colloid Interface Sci.* **1972**, *38*, 217.
(21) Evers, O. A.; Scheutjens, J. M. H. M.; Fleer, G. J. Statistical thermodynamics of block copolymer adsorption. 1. formulation of the model and results for the adsorbed layer structure. *Macromolecules* **1990**, *23*, 5221−5233.
(22) Fleer, G. J.; van Male, J.; Johner, A. Analytical approximations to the scheutjens-fleer theory for polymer adsorption from dilute solution. 1.trains, loops, and tails in terms of two parameters: the proximal and distal lengths. *Macromolecules* **1999**, *32*, 825−844.

https://dx.doi.org/10.1021/acs.macromol.0c00361
Macromolecules 2020, 53, 3900−3906